Straight talk- Shelikof Strait winds as revealed by buoy observations, SAR imagery and WRF simulations

John Papineau, NWS, Anchorage, January 2010

Introduction:

Strong winds in Shelikof Strait are a fairly common occurrence and at times impede and/or generate hazardous conditions for marine and aviation traffic. Figure 1 is an example of SAR imagery of northeast flow down the strait in conjunction with strong winds along the south coast of the Kenai Peninsula and southern Cook Inlet. At the time of the image (Dec 28, 2005) the winds at buoy 46077 (B77) were on the order of 15 ms^{-1} and 17.5 ms^{-1} at Amatuli Island (AMAA2).

Buoy 46077 was installed in autumn 2005, however since that time there have been significant periods during which the wind sensors have been inoperative or data has not been collected. At the time of this study there is a little under three years of data that can be analyzed. In addition, data from the C-Man station located 173 km to the north of B77 on Amatuli Island (AMAA2), near Kennedy Entrance is use to estimate the along-strait pressure gradient and to compare wind speed and direction. There are some important differences that should be noted between these two stations. First, the wind sensors at both platforms collect data every second; however the winds that are reported at B77 are an eight minute average, while those at AMAA2 are a two minute average (what will be referred to as sustained speeds). Both set of sensors use a five second average during the observation (eight or two minute) period to calculate gusts. Peak gusts, if reported (in the continuous wind file), is the strongest five-second average during the preceding hour. The anemometer on buoy 46077 is located approximately 5 m above the surface of the water. AMAA2 on the other hand is located on a rocky island with the anemometer at a height of 49 m above water level.

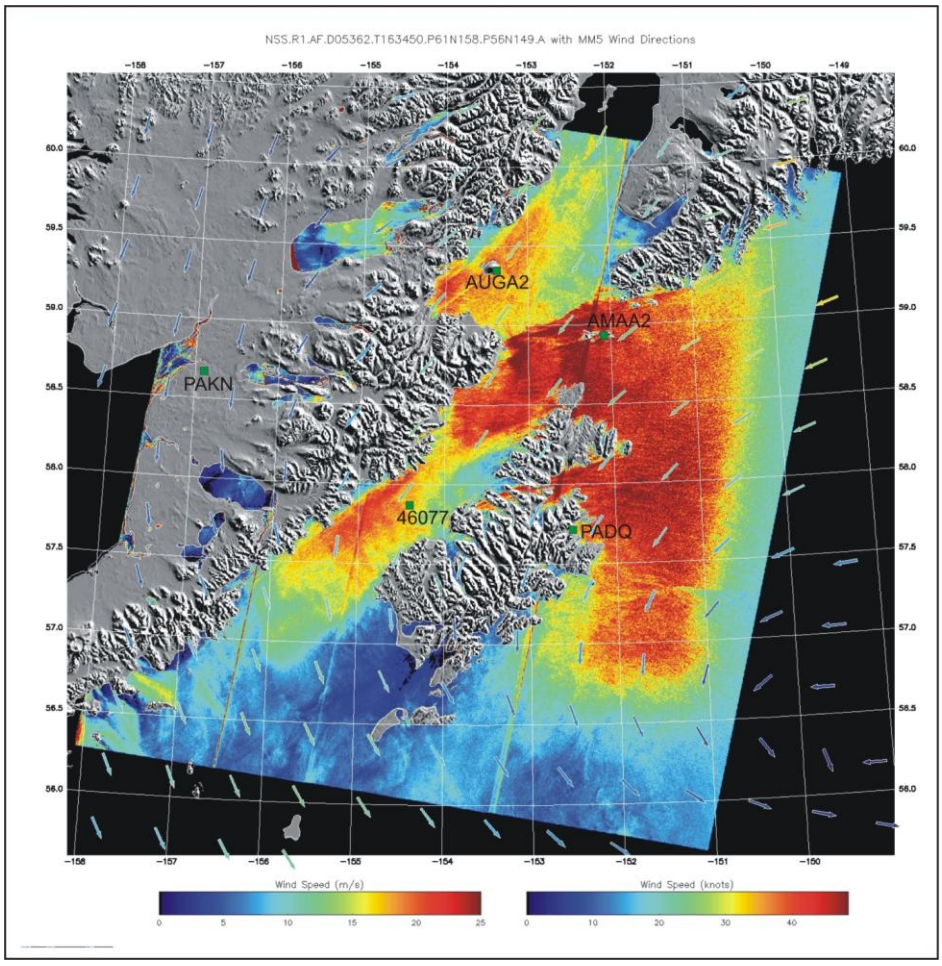

Figure 1: SAR imagery from December 28, 2005

A straight comparison of wind speeds between B77 and AMAA2 is not realistic because of the two different averaging periods and the greater height of the anemometer at AMAA2. In other words, all else being equal, the wind speeds at AMAA2 will appear to be stronger than at B77 by some unknown factor. Although no competitive analysis is attempted in this study, a reasonable estimate suggests that speeds at AMAA2 are 10-20% higher. This becomes important when we directly compare wind speeds at the two stations in order to estimate any acceleration that may have occurred due to ageostrophic forcings (i.e.- a 12 ms^{-1} wind at AMAA2 is probably equal to 10 ms^{-1} at B77).

Winds within and around Shelikof Strait can be broken down into several flow regimes, the most prominent are: 1) Northeast-North; 2) West-Southwest; and 3) Northwest. These different wind directions produce varying responses in terms of wind, waves, precipitation and at times superstructure icing.

Northeast-North:

Analysis of B77 data showed that there have been 28 events (listed in Table 1) during which the three hour averaged sustained winds were 18.0 ms^{-1} or higher. These events are listed in order of sustained speeds with accompanying data. Similar data from AMAA2 is listed when available. Since the orientation within the northern half of Shelikof Strait is approximately 40° with respect to true north, for analysis purposes any three hour average direction had to lie between 10° and 70°. These 28 events occurred within 12 different storm systems. Three hours was selected as the averaging criteria in order that the orientation of mean sea-level pressure field within the strait could be obtained from the North American Regional Reanalysis (NARR) data set.

The main results of this analysis are: 1) the five-second averaged gusts at B77 tend to be 23% higher than the eight-minute sustained speeds.

Table 1: 28 strong NE wind events

Date & Time	B46077			AMAA2			Press. grad. (mb 100km^{-1})	Isobar orientation (NARR data set)
	Wind Dir.	Speed (m/s)	Gusts (m/s)	Wind Dir.	Speed (m/s)	Gusts (m/s)		
Nov 15, 2005 5-7Z	038	21.8	26.6	042	22.6	26.1	3.3	SW-NE
Feb 9, 2008 17-19Z	042	21.2	26.7	—	—	—	—	W-E
Nov 15, 2005 2-4Z	040	20.9	25.1	049	21.5	25.0	3.7	Slightly SW-NE off of W-E
Dec 27, 2006 20-22Z	049	20.8	25.4	054	26.0	30.1	5.6	Primarily N-S
Oct 21, 2005 6-8Z	047	20.8	26.5	040	18.4	21.9	2.7	SW-NE
Feb 9, 2008 20-22Z	032	20.8	25.6	—	—	—	—	W-E
Nov 15, 2005 8-10Z	040	20.7	25.2	033	17.2	20.0	2.4	SW-NE
Dec 4, 2007 11-13Z	030	20.7	25.1	047	22.7	26.4	1.3	W-E
May 14, 2008 20-22Z	038	20.2	24.4	—	—	—	0.8	SW-NE
Feb 9, 2006 16-18Z	046	20.1	24.1	051	28.6	33.9	4.6	Slightly SE-NE off of W-E
Feb 9, 2008 14-16Z	046	20.0	24.1	—	—	—	—	W-E
Nov 25, 2007 18-20Z	067	19.9	25.0	063	24.0	30.1	5.4	NW-SE
Dec 27, 2006 17-19Z	055	19.7	23.8	055	22.9	27.4	5.7	N-S with slight SW-NE
May 14, 2008 17-19Z	040	19.6	24.6	—	—	—	1.8	SW-NE
Dec 27-28, 2006 23-1Z	044	19.5	24.2	047	28.1	33.8	4.8	NW-SE
Feb 9, 2008 5-7Z	046	19.5	23.9	051	21.7	26.1	3.1	W-E
Dec 10, 2007 14-16Z	046	19.5	23.3	063	21.8	28.5	3.2	W-E
Apr 5, 2007 18-20Z	048	19.5	24.0	—	—	—	3.3	W-E
Feb 16, 2008 21-23Z	028	19.3	24.5	045	25.4	34.2	-1.7	SW-NE
Feb 17, 2008 18-20Z	032	19.3	23.9	—	—	—	2.2	W-E
Dec 31, 2005 1-3Z	037	19.2	23.7	055	17.1	20.5	3.1	SW-NE
Feb 9-10, 2008 23-1Z	034	19.0	23.6	—	—	—	—	SW-NE
Oct 21, 2005 9-11Z	039	18.8	23.1	017	13.0	15.3	1.7	SW-NE
Nov 14-15, 2005 23-1Z	040	18.7	23.5	044	19.5	22.7	4.1	W-E
Dec 27, 2006 14-16Z	069	18.5	22.4	054	19.9	23.7	5.6	Weak pr. grad in NARR
Dec 28, 2005 1-3Z	038	18.5	22.6	031	16.0	18.4	2.2	W-E
Dec 14, 2005 5-7Z	064	18.4	23.6	081	18.3	21.6	4.9	NW-SE
Feb 9, 2006 13-15Z	056	18.0	23.0	063	21.7	25.7	5.2	W-E

Figure 2: wind speeds

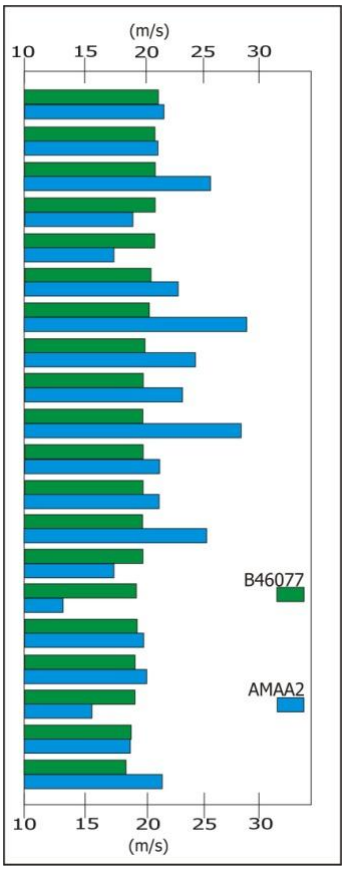

The low gust-to-sustained ratio would indicate that the environment is less turbulent when compared to other strong wind regimes such as downslope windstorms for example; nevertheless turbulence does exist as noted in the study of Lackman and Overland (1989) in which surface friction and entrainment into the top of the boundary layer are cited as the main sources.

2) As seen in Figure 2 the sustained wind speeds at AMAA2 during the same period can be significantly higher (3 events), similar (16 events) or significantly weaker (1 event) than the winds at B77 (AMAA2 winds were only available for 20 of the events). The 20 event mean wind speed at AMAA2 was 21.3 ms^{-1} compared to 19.8 at B77. 3) Inspection of the NARR data set for each event indicates that 13 events had W-E isobar orientation over Shelikof Strait and the Barren Islands, nine events had a SW-NE orientation, three were NW-SE, two were N-S. The Dec 27, 2006 event at 15Z had virtually no pressure gradient over the strait, which did not match the 5.6 mb 100 km^{-1} derived from the buoy data set. 4) Of the 12 storm systems represented by the 28 events, only three had centers that were west of Shelikof Strait, while the remaining nine had the low positioned south or east of Kodiak Island. 5) Inspection of SAR imagery and the NARR data set indicates that the main forcing for strong NE winds within Shelikof Strait are frontal jets (aka: low-level jets) that extend from south of the Kenai Peninsula through the Barren Islands and into the strait. 6) Wave heights during these events are of course a function of wind speed, duration, and fetch. Observations show that 4.5 m is about the maximum obtainable value for these types of events at the buoy.

One of the main topics of discussion in previous work has been the importance of gap dynamics in wind acceleration. For the majority of the 28 events acceleration of the winds due to gap dynamics appears to be minimal. This is born out by the data shown in Figure 3, in which the relationship between the down strait pressure gradient between AMAA and B77 is high variable. For individual events the speed at B77 versus pressure gradient displays considerable hysteresis- for a given pressure gradient speeds are lower when the event is developing compared to when it is diminishing. For example, in the Dec 10, 2007 event, with

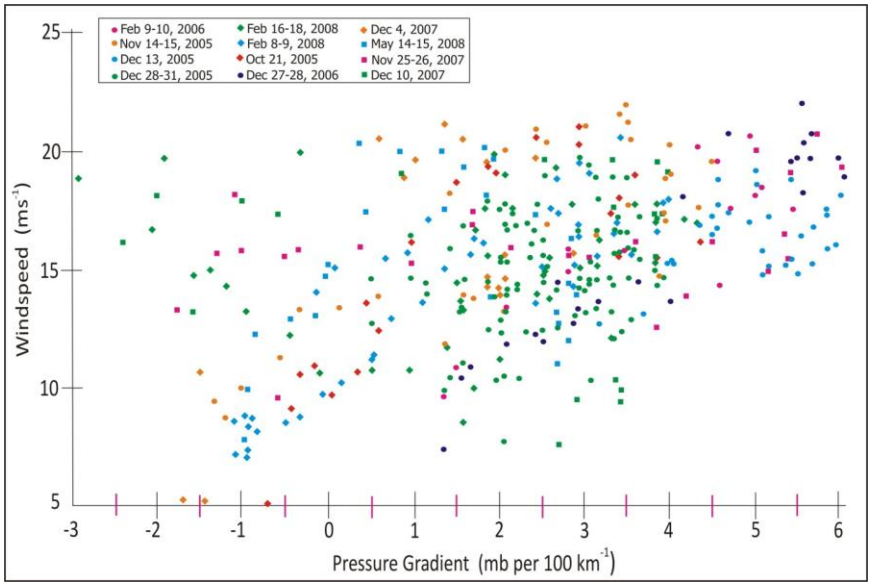

Figure 3: wind speeds at B77 versus pressure gradient.

a 3.8 mb 100 km^{-1} pressure gradient and the winds increasing, the speed at B77 was 15.8 ms^{-1}, five hours later as speeds and pressure gradient on the decease, at 3.8 mb 100 km^{-1} the speed was 19.5 ms^{-1}. In fact at times the pressure gradient can go negative (Nov 26, 2007; Feb 17, 2008, Dec 4, 2007) as the orientation of the isobars become N-S which occurs when a low center moves into the northern Gulf of Alaska. For the three NW-SE events the average pressure gradient was 5.0 mb 100 km^{-1} compared to 2.1 mb 100 km^{-1} for the nine SW-NE events.

When a frontal jet is the primary forcing for strong NE winds, the existence of the gap produced by Shelikof Strait is of minor importance. In other words strong winds of a similar magnitude would form even if Kodiak Island did not existence; as they do along the entire Gulf of Alaska coast that is ringed by high mountains (Liu *et al* 2006). When a frontal jet is absent or weak and the orientation of the isobars is W-E or NW-SE along-strait acceleration becomes important. The magnitude of the acceleration cannot be determined by the sparse observations. This question is addressed in a following section where a series of high resolution WRF model simulations are discussed.

Southwest:

Strong flow through the strait from the southwest is less frequent when compared to NE events. In fact, there are only two events (Feb 15, 2008; 5-7Z and 2-4Z) where the wind speeds are 18 ms^{-1} or stronger. It should be noted that the typical wind direction at B77 for these events is 250^{o}-260^{o} compared to an along-strait orientation of 220^{o}. This is a result of the fact that many of events involve cold air drainage through the Aleutian Range. During the Feb 15, 2008 event cold air was pooled over the eastern Bering Sea with significantly warmer air east of the Alaska Peninsula. Air temperatures at B77 cooled from -6^{o}C to -12^{o}C as the wind speed slowly ramped up to 20 ms^{-1} over a nine hour period. The wind direction during this time was consistently from 250^{o}. This was a result of a 984 mb low located over the Kenai Peninsula coincident with a 1005 mb high over the southern Bering Sea. The NARR data set shows NW-SE orientation of the isobars over the strait. The consistent westerly component (250^{o}-260^{o}) to the winds instead of an along-strait component (closer to 220^{o}) is a product of the gap flow. Air flowing into the southern half of Shelikof Strait has two sources: the area directly to the south around the Semidi Islands, and Bristol Bay. At times, depending on the orientation of the isobars, air can originate from one source area more than the other. It would appear that a considerable portion that flows past B77 originates in Bristol Bay and crosses

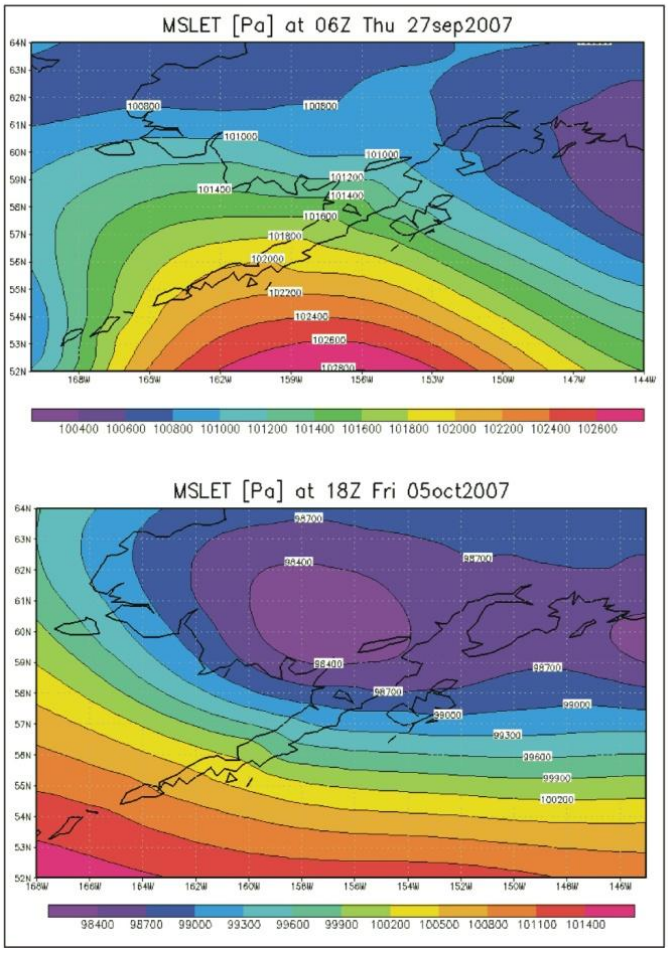

Figure 4: MSLP from the NARR data set.

the Alaska Peninsula via Becharof Lake (W-E) and then backs toward the NE as it enters Shelikof Strait from Pulae Bay to Kashvik Bay. Wave heights at B77 for the Feb 15, 2008 event reached a maximum of 4.1 m, a direct indication that a swell from the SW-S had entered the strait. For comparison the winds at AMAA2 during this period were NW at 4 ms^{-1}.

Another similar event occurred on October 5, 2007 where a low centered in Southwestern Alaska produced W-E isobars over Shelikof Strait. Over a 10 hour period the winds at B77 ranged from 225° to 267° with the speeds ranging from 15.0 ms^{-1} to 17.4 ms^{-1}. Maximum wave height reached 4.1 m, once again indicating that a northeast traveling swell from the North Pacific had entered the strait. Winds at AMAA2 at the same time were on the order of 14-18 ms^{-1} from 250°.

Figure 4 shows the MSLP field for two SW events. On September 27, 2007 a high was positioned south of Chignik (PAJC), the flow at B77 averaged 13 ms^{-1} at 250°, maximum wave height was 2.6 m. The second example is taken from October 5, 2007 where a low centered in Southwestern Alaska produced W-E isobars over Shelikof Strait. Over a 10 hour period the winds at B77 ranged from 225° to 267° with the speeds ranging from 15.0 ms^{-1} to 17.4 ms^{-1}. Maximum wave height reached 4.1 m, once again indicating that a northeast traveling swell was an important component. Winds at AMAA2 at the same time were on the order of 14-18 ms^{-1} from 250°. Maximum wave height reached 4.1 m, once again indicating that a northeast traveling swell was an important component in the second event but not the first.

The majority of SW events tend to occur with moderate wind speeds ranging from 12-15 ms^{-1}. This is the case because gap acceleration is an important component, or at times the primary component. In contrast as noted in the proceeding section, frontal dynamics dictate the stronger NE events, with gap dynamics playing a secondary role.

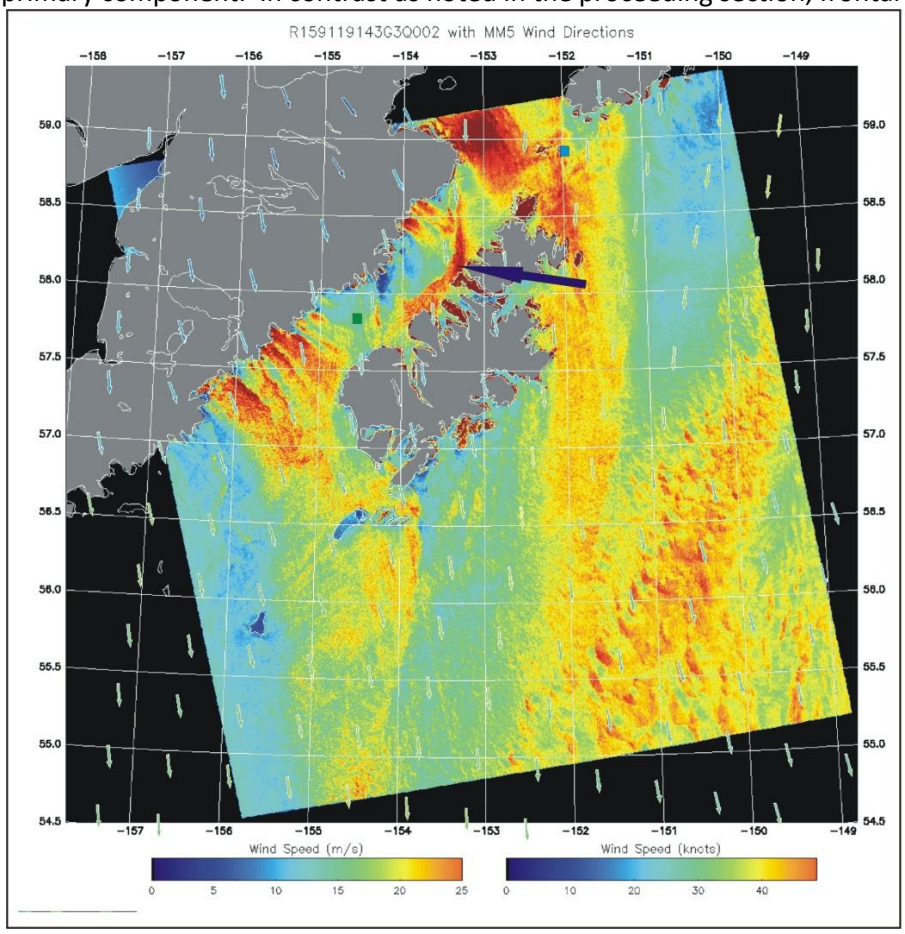

Figure 5: SAR image of NW flow across the Alaska Peninsula.

Northwest:

Strong NW winds that flow through Shelikof Strait perpendicular to the long axis are a common occurrence during the cooler months of the year (Nov-April). Localized winds can be very strong (>20 ms^{-1}) with gusts exceeding 30 ms^{-1} near gaps in the upstream terrain. The major concern for mariners besides the strong winds is the potential for significant superstructure icing. When a cold airmass resides over western Alaska and the eastern Bering Sea, cold

air flows through the gaps in the Aleutian Mountains. The resulting accelerated outflow can be oriented either W-E or NW-SE, and often changes as the synoptic weather pattern evolves. Once inside the strait, NW winds for example either flow on a straight course across the width of the strait or in the event of an N-S pressure gradient, the air will curve to the south. Westerly flow into the strait can in a similar fashion move directly across or curve northward or southward. B77 rarely displays NW moderate to strong winds, if they appear they are short lived as the wind direction transitions to either N or W. January 27-28, 2006 is a case were B77 did maintain moderate (12-14 ms^{-1}) NW winds for a number of hours while a low was positioned over the northcentral Gulf of Alaska. Air temperatures dropped to -13.8^{o} C which is the coldest recorded value at the buoy to date. The B77-AMAA2 pressure gradient reached a maximum around 5.0 mb early on the 28th; although no SAR imagery is available at this time, we suppose that the moderate NW flow across the region superseded up-strait flow as indicated by the pressure gradient; this does not preclude some backing of the NW winds toward the W due to this low-level pressure field. Figure 5 shows SAR imagery for the NW flow case for March 10, 2007. Outflow from the various gaps in the Aleutian Range is apparent as is the absence of moderate to strong winds for the majority of the middle section of Shelikof Strait. The exception is the band of stronger winds indicated by the purple arrow: the flow was initially from the north but by mid-strait is out of the NE. At this time a 985 mb low was centered about 250 nm east of Kodiak Island. Although data from AMAA2 is missing, there was most likely a weak down the strait pressure gradient.

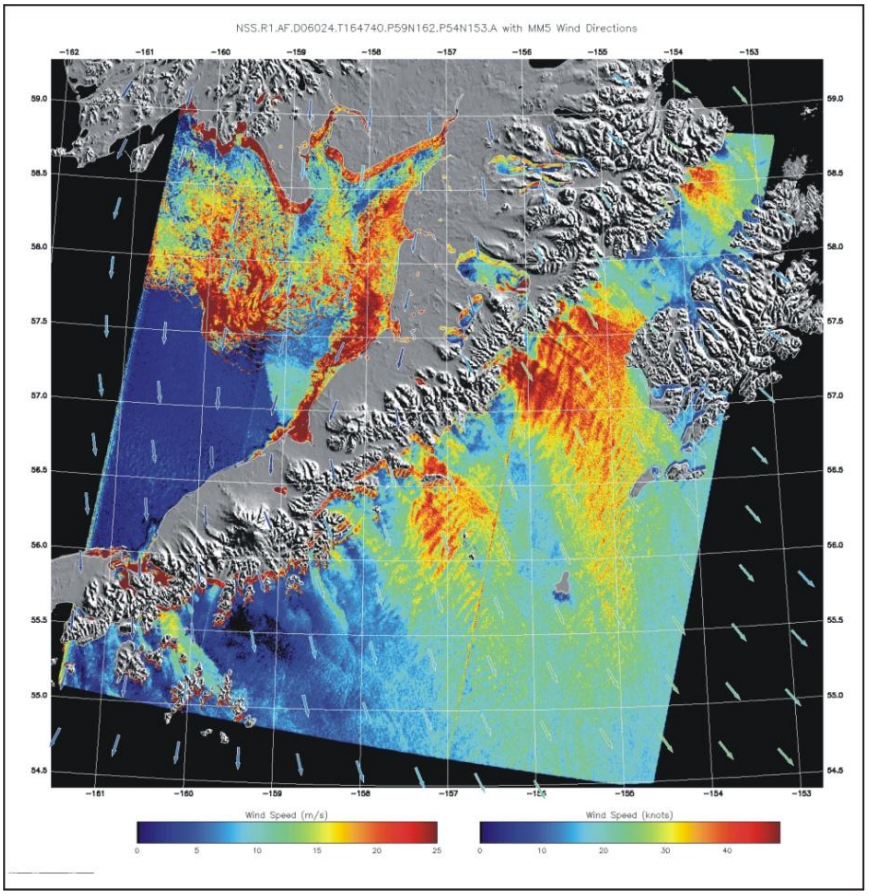

Figure 6: SAR image of NW flow across Alaska Peninsula with downstream gravity waves.

Although not present in the March 10, 2007 image, a significant number of NW flow cases display gravity-wave patterns downstream of the Aleutian Range as seen in Figure 6. Although SAR instrumentation measures micro-scale surface roughness, atmospheric gravity waves often produce these patterns on the surface of the water (Young *et al* 2006). The difference between gravity wave and non-gravity wave cases is the depth of the NW flow, stability of the lower troposphere as well as wind speeds at mountain crest level. As noted by Bond & Macklin (1993) in their study of winds in and around Wide Bay, these gravity waves can produce localized areas of lower pressure within 10-50 km of Aleutian Range which in turn may provide additional accelerate in boundary layer coastal winds, including those in Shelikof Strait. Flows characterized by atmospheric gravity waves are not necessarily

stronger or extend further downstream then their shallower counterparts; nevertheless the potential for areas of downslope winds to the lee of the Aleutian Range exists.

Discussion of Observations:

Figure 7 shows the frequency of winds of a given speed segregated into eight directional sectors. It is clear that the NE regime dominates at both moderate (≥12 ms^{-1}) and strong (≥18 ms^{-1}) wind speeds. This result reflects the nature of the synoptic weather patterns across the region in which intense low pressure systems centers tend to occur more frequently in the Gulf of Alaska than in the eastern Bering Sea. The sheltering of B77 from W-NW winds by the Aleutian Range also should be considered but is of secondary importance. Comparison of wind speeds at AMAA2 with B77 and inspection of NARR MSLP fields indicates that the highest wind speeds during the NE regime occur when a coastal/frontal jet extends at least into the northern part of Shelikof Strait. The enhancement of wind speeds by a along-strait pressure gradient during these events is minimal although one can neglect some degree of acceleration due to mass convergence within the confines of the strait (Liu et al 2006). It was also noted that the AMAA2-B77 pressure gradient can only be used as a viable estimate of wind speeds within the lower half of the strait when gap dynamics are prevalent.

Essentially the flow in Shelikof Strait during the strongest NE events can be thought of as an extension of the interaction of frontal jets and steep terrain that rings the entire Gulf of Alaska (flow along an open steep coastline). It should be noted however in the absence of a coastal/frontal jet, acceleration of the winds due to an along-strait pressure gradient is important, but cannot be quantified from the current data set. Although not investigated in this current study, gap dynamics is probably more important for more modest wind events (absence of frontal jet), as illustrated by the case study of Lackmann & Overland (1989). A series of high resolution mesoscale model simulations would hopefully shed light on this question. It is certainly possible that a mixture of frontal and gap dynamics can occur as well, especially in southern half of the strait near the exit region.

Southwest flow through the strait occurs more frequently than B77 indicates because of the channeling affect of the winds from this direction. Despite modest wind speeds when compared to the NE regime (at least as observed at B77), during SW regimes significant wave heights can be established within the strait due to the propagation of a large swell from the North Pacific. Cold advection into Shelikof Strait via W to N winds is underrepresented in Figure 7 because B77 is located in a position

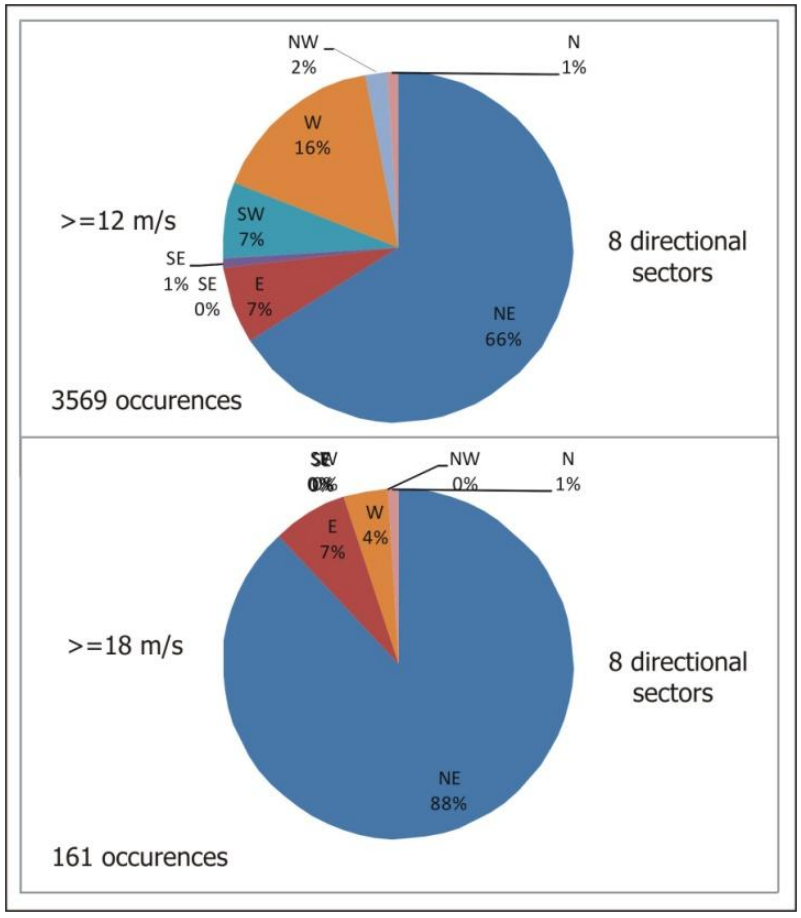

Figure 7: Frequency of flow by direction.

that is sheltered to a large degree from NW winds. Air temperatures in the strait can drop 5-10° C over a six hour period and remain well below freezing for extend periods. Cold air and moderate to strong winds generates areas of superstructure icing. SAR imagery reveals the detailed nature of outflow from gaps in the Aleutian Range during cold events, the potential for downstream lee trough due to atmospheric gravity waves also adds a level of complexity to the resulting low-level wind field. In essence, the complexity of various flow regimes cannot be captured by a simple two station analysis of winds and pressure as presented in this paper, only broad generalizations should be referenced.

WRF Simulations:

In order to gain a deeper insight into the nature of Shelikof Strait winds five mesoscale simulations were conducted using the WRF model; however the results from only two of the simulations are presented below in detail because of overlapping characteristics. The model was initialized and nudged using 3-hourly NARR boundary files. A single 4-km grid was used for the model domain; 4-km was judged sufficiently high enough resolution for the primary terrain features. Figure 8 shows the model terrain, it is important to note that although the width of the strait (perpendicular to along-strait axis) at sea-level varies from 40-50 km. If we consider the width at some elevation above sea-level, in this case at 200 m, the strait narrows around 58°N. This is clearly shown in Figure 8b where the across-strait width in the northern half varies from 60-90 km but narrows to 45 km in the southern half.

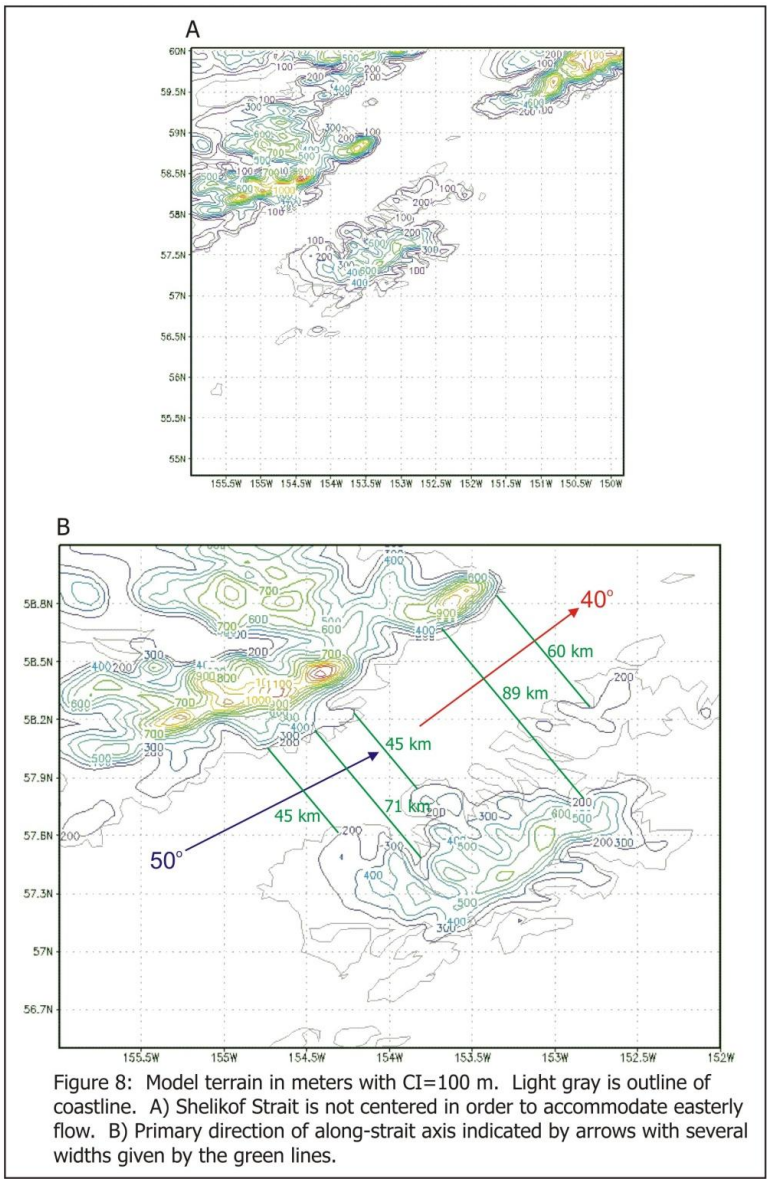

Figure 8: Model terrain in meters with CI=100 m. Light gray is outline of coastline. A) Shelikof Strait is not centered in order to accommodate easterly flow. B) Primary direction of along-strait axis indicated by arrows with several widths given by the green lines.

December 27-28, 2006:

This event is worthy of closer examination because over the course of time it represents three different flow regimes; in addition, the wind speeds at AMAA2 were some of the highest to be recorded since the inception of the C-man station. The simulation was initialized at 00Z/27 and run through 06Z/28. Modeled wind speeds and direction match B77 quite well with the exception of 00Z/28 at which time the model field tends to reduce the speeds two to three hours too quickly.

Synoptically a 978 mb low was positioned in the

eastern Aleutians at 12Z/26 but by 00Z/27 had deepened to 971 mb and was just south of the southern tip of the Alaska Peninsula. In addition, the low center became elongated with a lobe extending NE to the Semidi Islands. This secondary feature was critical because it enhanced the pressure gradient within Shelikof Strait. Over the subsequent 24 hours the low slowly weakened to 983 mb and was now centered south of Cold Bay, the elongated center remained relatively stationary until early on the 28th when it began to translate toward the northwest. A deep low was forming in the southern Gulf of Alaska late on the 27th but had no impact on this event. An equally important component to this event is the existence of a warm or occluded front and accompanying strong (35-40 ms^{-1}) low-level jet that moved over southern Kodiak Island around 12Z/27 and over the Barren Islands at 21Z/27. It was while the LLJ was positioned over the Barren Islands that the wind sensor at AMAA2 recorded a sustained speed of 30 ms^{-1} with gusts in excess of 34 ms^{-1}.

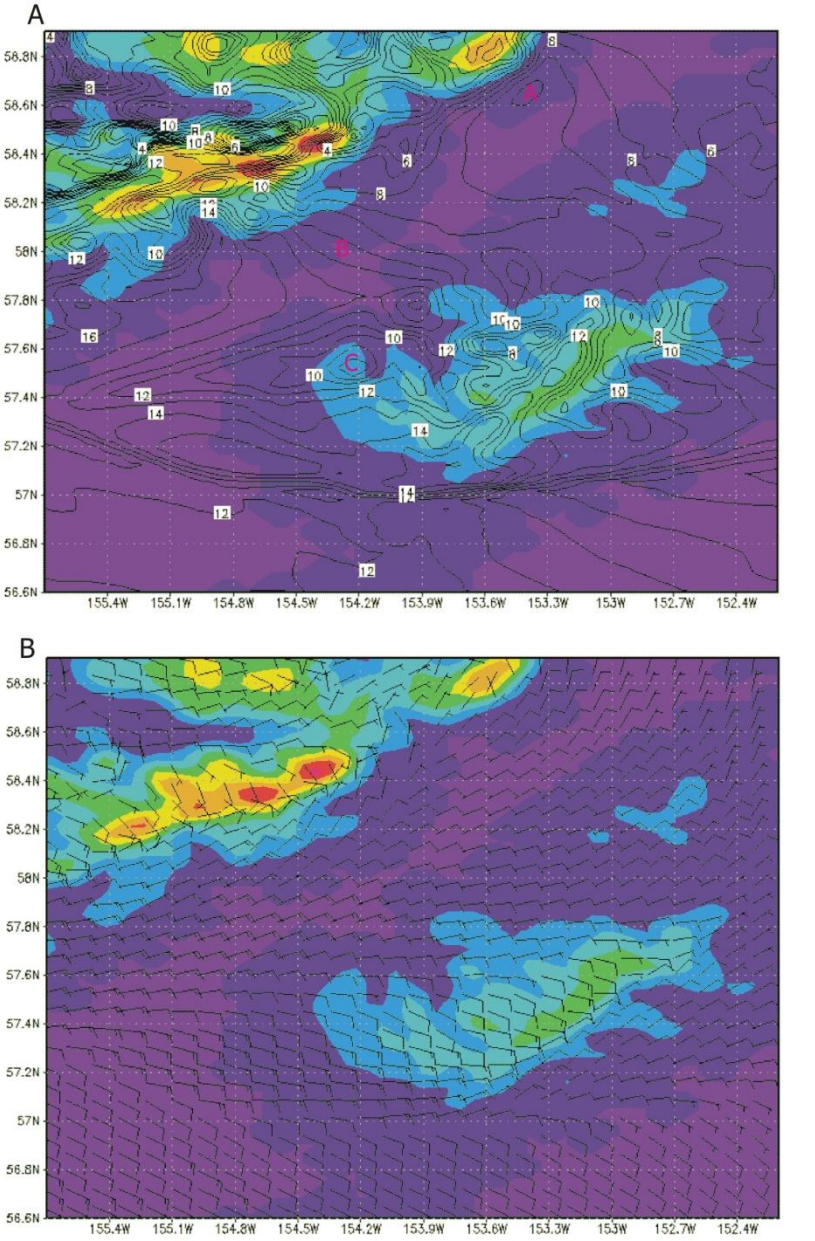

Figure 9: A) wind speeds with CI= 1m/s and every other contour labeled. B) Wind barbs (full flag is 10 m/s). Valid 04Z December 27, 2006.

The three different flow regimes are as follows: 1) Along-strait NE flow due to pressure channeling with the strongest winds in the narrowest part of the strait near 58°N (00Z-09Z/27). 2) Moderate-to-strong east flow across Kodiak Island as the LLJ migrates northward (10Z-16Z), with no preferred area of strongest winds. 3) Strong NE in the strait with strongest winds in the northern sector and considerable deceleration to the south (17Z/27-06Z/28). It is important to keep in mind however that there are considerable across-strait variations in wind speed, direction as well in the pressure field.

Figure 9 shows a plot of the lowest model level wind speeds during the first regime (04Z/27), with the light blue shading indicating the 200 m elevation contour. Note that in the upper strait there is

weak flow convergence as air enters from Cook Inlet (northerlies) and from east of the Barren Islands (northeasterly). The area labeled 'A' is a small wind maxima due to flow around the higher terrain of the Fourpeaked Massif (Fourpeaked Mt. and Mt. Douglas). The majority of acceleration, from 8 to 14 ms^{-1}, occurs at 'B' where the across-strait width decreases. In order to understand the importance of mass flux convergence within the strait (Gabersek & Durran 2006), two control volumes were established (not shown), one in the northern sector and the second in the south. Analysis indicates that mass is accumulating with the strait at this time, even in the southern control volume where the speed in the exit region is 65% higher than in the entrance. The additional mass is coming from weak-to-moderate easterly flow over Kodiak Island. Detailed analysis is difficult due to the irregular nature of the terrain and the non-steady flow. In the center of the strait the flow is from the NE as one would expect in a 'pure' pressure gradient driven flow, however on the sides mass is entering the strait at an oblique angle. The acceleration at 'B' is therefore a result of both the narrowing of the channel complemented by mass convergence upstream of the constriction. In addition, the base of the inversion in the northern half of the strait is on the order of 850 m but across the constriction lowers to about 500 m. Another way to look at this is that the 271^{o} isotherm starts at an elevation of 950 m north of the constriction but lowers to the surface 100 km to the south. Therefore the terrain constriction not only effectively forces horizontal convergence but also is a favored location for vertical convergence as well since the base of the inversion acts in a first order approximation as a material surface (Lackmann & Overland 1989). The lowering of the inversion at the constriction is a function of the acceleration of the flow which in turn requires that mass be conserved.

The area labeled 'C' indicates a speed minimum due to flow around and over the terrain of Kodiak Island (more on this next). One important point to note that the cross-strait flow pattern is asymmetrical throughout most of the simulation as will become apparent when the other two flow regimes are discussed.

The second regime is characterized by moderate-to-strong easterly flow from the surface through 800 mb, in conjunction with the northward movement of the LLJ in the western Gulf of Alaska. Figure 10 shows two examples from this easterly regime at the lowest model level. In Figure 10A the flow within the strait is primarily NE-SW, two hours later however (Fig 10B), with minimal apparent changes in the

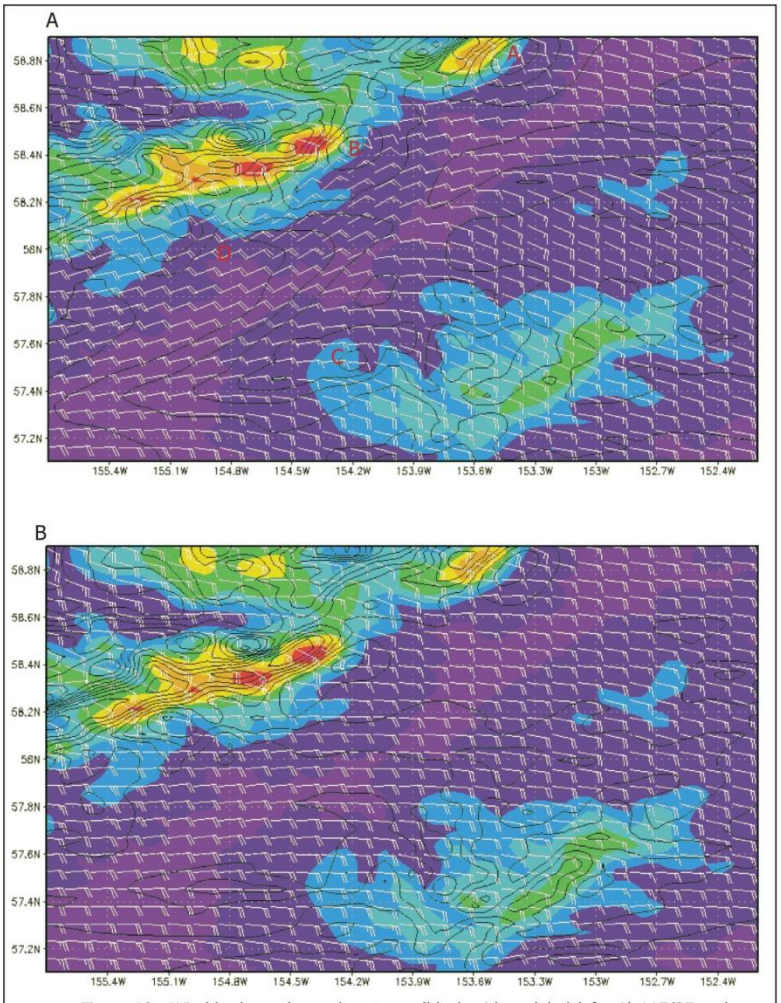

Figure 10: Wind barbs and speed contours (black with no labels) for A) 11Z/27 and B) 13z/27.

upstream flow, directions within the strait have veered and become easterly. This change is due to a significant decrease in low-level stability (the Brunt-Vaisala frequency decreased dramatically) due to warm advection in the surface to 900 mb layer with little change in temperatures above this layer. The net result was a decrease in blocking over the two hour period as seen in the areas labeled 'A' and 'B'. A speed minima at 'C' in Figure 10A is a result of a lee-side wake; although not clear in these large-scale plots, the flow pattern to the lee of Kodiak Island (west coast in this case) and adjacent portion of the strait, is a function of mountain waves that form over the higher terrain of the island as well as the gaps in the terrain. A boat seeking safe anchorage within the multitude of bays and coves on the West Coast would have to judiciously select the appropriate one as some locales would actually experience higher wind speeds then areas within Shelikof Strait. The area labeled 'D' is a speed maxima resulting from two processes: 1) flow down the western half of the strait is stronger due to flow convergence, and; 2) flow over and down the 500 m high terrain northeast of Katmai Bay is undergoing considerable local-scale acceleration due to downsloping (clearly illustrated in potential temperature field).

The third regime is seen in Figure 11 where the lowest model level wind barbs are valid during a time when the LLJ was positioned over the Barren Islands. The area marked with an 'A' has the highest low-level wind speeds; with strong easterly flow over the northern half of Kodiak Island. Although it is difficult to interpret from the plot, the winds in the middle of the strait are actually decelerating. The point 'B' indicates an area of strong NE winds which is essentially a coastal jet, which we have already mentioned is formed by the higher terrain of the Aleutian Range which is blocking easterly flow under stable lower-tropospheric conditions (Brunt-Vaisala ~0.013 in the 900-800 mb layer). A large wake labeled as 'C' is formed by the ascending limb of a mountain wave that is generated at 'D' by the easterly flow in the 900-800 mb layer.

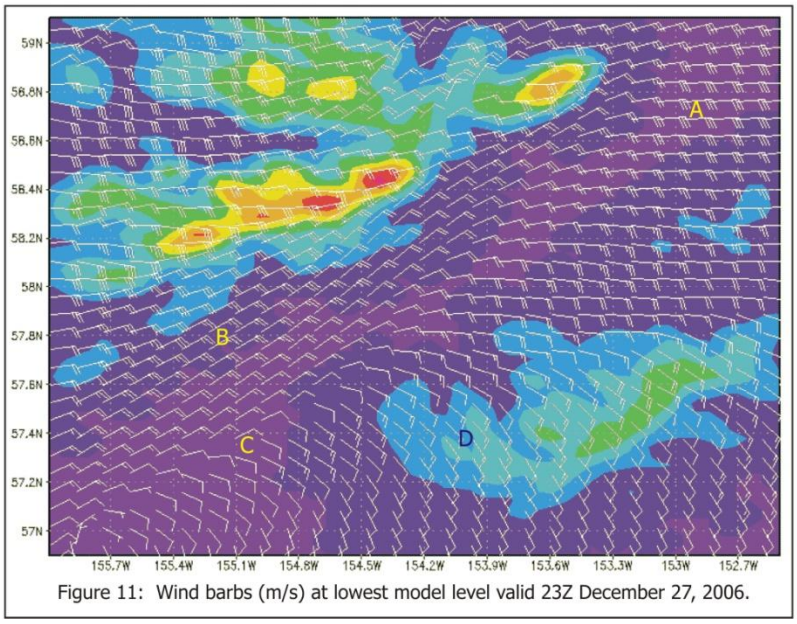

Figure 11: Wind barbs (m/s) at lowest model level valid 23Z December 27, 2006.

It is worthy of note that the level of maximum wind speed within the strait varies according to the regime: during pressure channeling the maxima tends to occur around 950 mb, roughly 500 m above the surface. When a LLJ and coastal jet are the dominate forcing maximum winds within the strait are typically in the 850-750 mb layer, 1500-2500 m above the surface. This of course has impacts on aviation through the region: pressure channeling is a near surface phenomenon while LLJ features can extend well into the middle troposphere. The presence of a LLJ is frequently associated with moderate-to-high amplitude mountain waves as air moves perpendicular to the higher terrain of Kodiak Island and the Aleutian Range.

January 24, 2006:

A 24 hour simulation of northwest winds was conducted using the same single 4-km domain as noted above. The SAR image of Figure 6 shows the flow pattern just prior to 17Z in which a significant portion of Shelikof Strait maintains weak winds but with northwest flow through the Aleutian Range.

Model output as seen in Figure 12 reveals the complex interplay between gap and downslope flow. For comparison B77 (located just NE of 'G' in Fig 12) during this period reported light (<5 ms^{-1}) and variable winds.

On the 4-km domain (Fig 12) there are three elevated gaps (A, C, D) in the Aleutian Range through which the winds are accelerated. The Kaguyak Gap labeled as 'A' is considerably wider than the other two and the mass flux through it is substantial: strong winds (≥ 20 ms^{-1}) extend three-quarters of the width of Shelikof Strait as seen at point 'B'. Rainbow Gap ('C') and Katmai Pass ('D') have strong winds within the gap but directly downstream gap winds merge with lee-side downslope winds, although discernable weak jets extend into the northwestern strait at 'E' and 'F'. An interesting characteristic of outflow from these narrow (15 km <) gaps is that the jets are a low-level feature, at least for this particular event they are only 500 m deep. Above this layer the ascending limb of the mountain wave (or hydraulic jump) and associated weaker winds merge laterally suppressing the depth of the jet. This property of lateral convergence of gap flow was noted by Gabersek & Durran (2004a) in their model simulations using idealized terrain.

The region labeled 'G' is one of very light wind that maintains an eddy structure throughout the simulation. Although not definitive it would appear that the large area of weak flow in the middle of the strait is due to the existence of the rising limb of a low-level mountain wave generated by the Aleutian Range (no wave breaking). Without the aforementioned gaps this entire section of Shelikof Strait would experience light and variable winds. Although the model is run using a 4-km grid, which

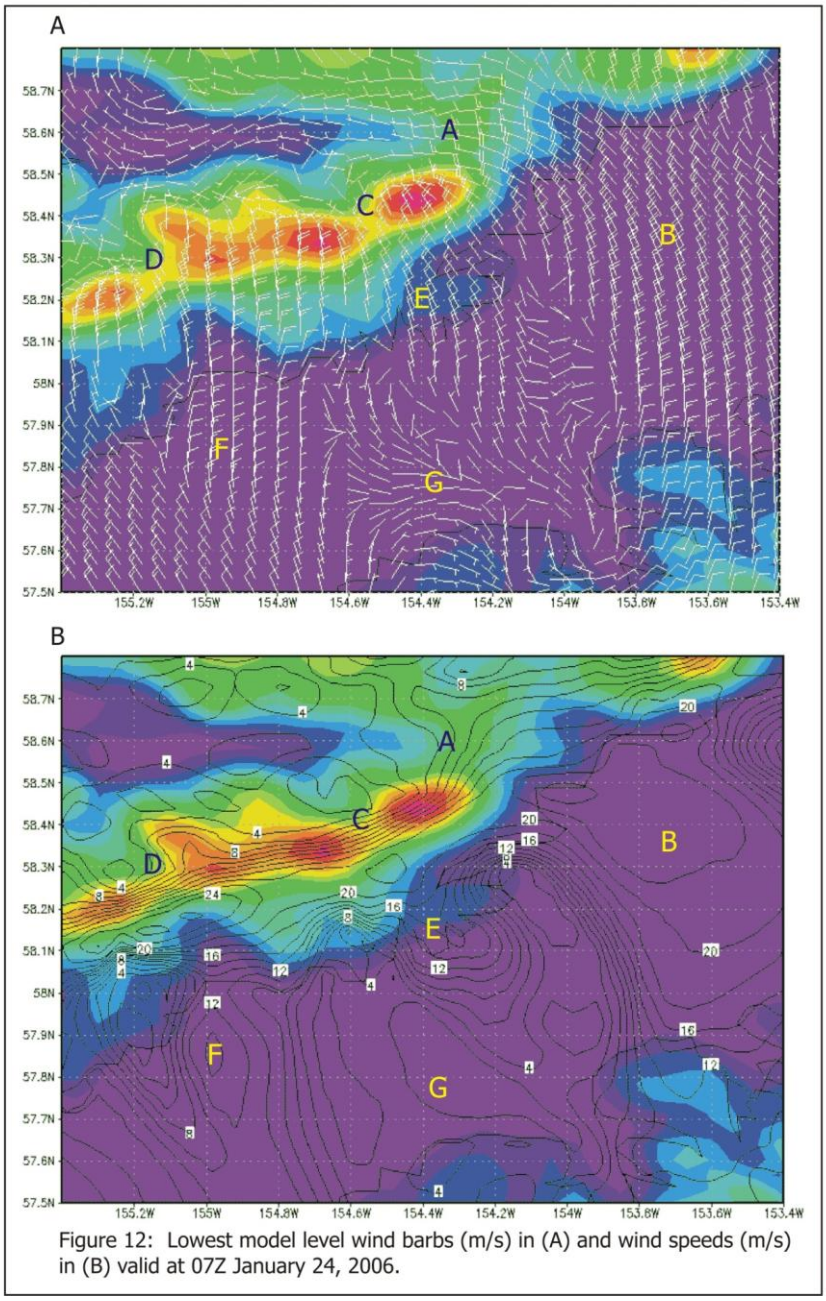

Figure 12: Lowest model level wind barbs (m/s) in (A) and wind speeds (m/s) in (B) valid at 07Z January 24, 2006.

does not resolve the smaller terrain features, the general idea is consistent. Any ship traveling the length of the strait would likely encounter areas of strong NW-W west winds and possibly freezing spray, intermixed with areas of light and variable winds.

In a second simulation of NW flow, January 20-21, 2001 (not shown) the movement of air through the gaps into the strait was clearly a result of the deep cold air that had pooled on the north side of the Aleutian Range. Early in the simulation the winds at crest-level were weak; the gap winds were a result of cold air drainage as the deep cold air formed a NW-SE pressure gradient. Later in the simulation as crest-level winds increased weak-to-moderate gravity waves formed to the lee of the higher terrain, including the elevated gaps; however they were considerable weaker than the waves generated during the January 24, 2006 event. This second example illustrates the fundamental point that two forcings of varying magnitude (strong versus moderate-weak mountain waves) may produce nearly the same magnitude response downstream. The model also shows that even in cases where weak mountain waves are produced, wakes form within Shelikof Strait.

It is interesting to note that the model generated breaking mountain waves (HJ) to the lee of the Aleutian Range produce maximum winds typically from one-half to three-quarters the distance down the lee slope. In the lowest model layers deceleration of the winds occurs just beyond the base of the mountain, where the air is no longer accelerated by gravity. This deceleration downstream of the terrain occurs despite a reduction in surface friction as the air is now moving over water. Above this thin layer the winds decelerate closer to the base of the mountain (i.e.- over the lower slopes). Whether these are real world features or model artifacts remains to be seen although such properties are noted by Durran (1986) in his modeling study using highly idealized terrain. Although not conclusive it is suggestive that entrainment from the turbulence generated in a HJ is entrained downward (air with lower momentum is forced to lower elevations) below the wave breaking region. How low and how far downstream in the model atmosphere wave breaking directly impacts wind speeds is difficult to discern. It would appear that the upstream portion of a wake is a result of low momentum air being mixed downward below the jump, additionally the presence of a reverse pressure gradient due to the cooling of air within the rising limb of the hydraulic jump probably has some impact as well. The downstream portion of a long wake appears to be the function of the advection of potential vorticity created by the HJ, as discussed by Schar (1993) and Smith *et al* (1997). In cases where a mountain wave is formed but no wave breaking, as for example in flow over a smooth ridge (elevated gap), local dissipation of the energy and deceleration of the winds will occur in some region above the surface, however shooting flow typically exists below this level.

Bond and Macklin (1993) in their study of winds in the vicinity of Wide Bay noted that their low-level aircraft flights revealed the existence of a pressure trough located in the southwestern part of the strait, just south of Puale Bay during periods of strong NW flow. They attribute this feature to a mountain wave that formed over the higher terrain of Mt. Martin-to-Mt. Mageik. In the current simulation the lee-side mesoscale pressure trough is located over the southern flanks of the ridge with no discernable mountain wave over the strait itself. What is of interest in the this region is the presence of a pressure ridge south of Wide Bay- which appears linked to the advection of cold air from the Bering Sea side of the Alaska Peninsula. This ridge extends from the surface through about 700 m. A strong outflow jet extends from the Puale-Wide Bay line downstream for about 100 km before it merges with the weaker ambient flow. The existence of the jet is due to the convergence of cold air through this ~75 km wide gap.

Although not within Shelikof Strait, for NW flow cases there is a consistent wake directly to the lee of Kodiak Island (not shown), typically centered near 57^{o}N/153^{o}W. The higher terrain of the island does generate a weak mountain wave but the bulk of the low-level winds are diverted around the north or south coasts, as a result the length of the wake is considerably shorter than the length of the higher terrain on the island.

Another interesting feature present in the simulated wind fields is the existence of a corner or tip jet just north of Cape Douglas near 58.9°N 153.2°W. Figure 13 shows the 1000 mb wind speeds and the 950 mb vertical velocities. The Fourpeaked Massif blocks a significant portion of low-level NW flow as seen in Fig13A; however some of the flow moves over the northern shoulder ('A') of the massif and accelerates as it descends the lee-slope. An elongated jet ('B') extends tens of kilometers downstream with a wake ('C') is clearly evident directly to the lee of the highest terrain. Another jet is indicated at 'D' as air moves out of the Kamishak Gap. The dynamics responsible for the creation of the two jets and wake differ and are briefly considered. The wake is created because strong acceleration down the lee slope forms a hydraulic jump (HJ) which is dissipative and introduces low momentum air from aloft into the lowest layers within the strait. Air flowing over the NE shoulder at 'A' also descends to the lee but does not terminate in a HJ, although a weak mountain wave does form. In the absence of the HJ the descending air maintains its momentum as it moves towards the Barren Islands (the flow is weakly supercritical). The 950 mb heights (not shown) indicate that there is a sharp height gradient from 'A' to 'B'. The curvature to the right as the flow reaches northern Kodiak Island is due to the down inlet pressure gradient and Coriolis deflection. The jet at 'D' is the outflow from the elevated gap that separates the Fourpeak Massif to the northeast and Mt. Martin to the southwest; there is evidence (not shown) that another tip jet forms to the NE of Mt. Martin which in turn accentuates the gap flow. The formation of strong low-level jets intermixed with wakes as important consequences for mariner. SAR imagery suggest that are preferred areas where jets including tip jets form; these features are a function of low-level upstream wind direction and speed, as well as stability and depth of the cold air (height of inversion). Subtle changes in these controlling parameters can alter the resulting jet structure significantly.

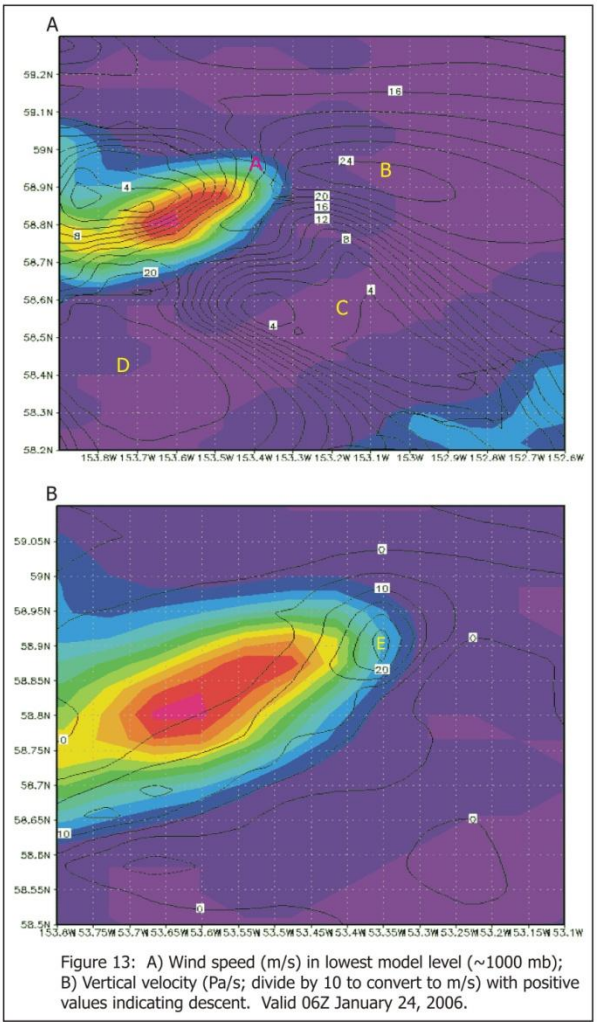

Figure 13: A) Wind speed (m/s) in lowest model level (~1000 mb); B) Vertical velocity (Pa/s; divide by 10 to convert to m/s) with positive values indicating descent. Valid 06Z January 24, 2006.

Summary:

WRF simulations of a number of different wind events in and around Shelikof Strait suggests that a considerable percentage of the along-strait and across-strait heterogeneity in the wind field is due to local blocking mountain wave generation by the terrain of the Aleutian Range and has less to do with traditional gap dynamics; chiefly mass convergence. Variations in wind speed maxima and minima are a

function of wind speed and direction and stability- hence as synoptic weather moves across the region, the flow within the strait evolves from one state to the next. The irregularity of the terrain on the Alaska Peninsula (sea-level and elevated gaps as well as irregularities of the coastline) generates multiple flow solutions over distances on the order of 10-30 km. In other words for strong SE-E flow across Kodiak Island, instead of one long continuous coastal/barrier jets, there are two or three mini jets as revealed by WRF simulations. These are not readily apparent in SAR imagery because they probably occur more frequently over land then over the water of the eastern strait. In contrast to the constantly evolving pattern during E flow, NW flow generates the most stable pattern in time although the spatial complexity is quite large. The existence of some of these mesoscale features produced by the model need to be verified by mariners and aviators.

Appendix A:

Since the blocking of low-level flow by the higher terrain of the Aleutian Range is a common occurrence along Shelikof Strait a detailed investigation is warranted. Results from numerous WRF simulations indicates that the region east of the Fourpeaked Massif is one of frequent blocking due to the high incidence of moderate-to-strong east flow through Kennedy Entrance. The following analysis is based on the Dec 27, 2006 event, particularly on the 13-23Z period during which time lower tropospheric easterly flow increased from 16 ms^{-1} to over 30 ms^{-1} as the LLJ moved directly over the Barren Islands. In addition there was significant warm air advection (~6^{o}C) into southern Cook Inlet and northern Shelikof Strait that played an important role in the blocking regime.

In general, blocking is a function of terrain height, wind speed, wind orientation with respect to the terrain, and lower tropospheric stability. Changes in one or more of these parameters can produce noticeable modifications in the severity of blocking. The ultimate manifestation of blocking is stagnation accompanied by flow reversal.

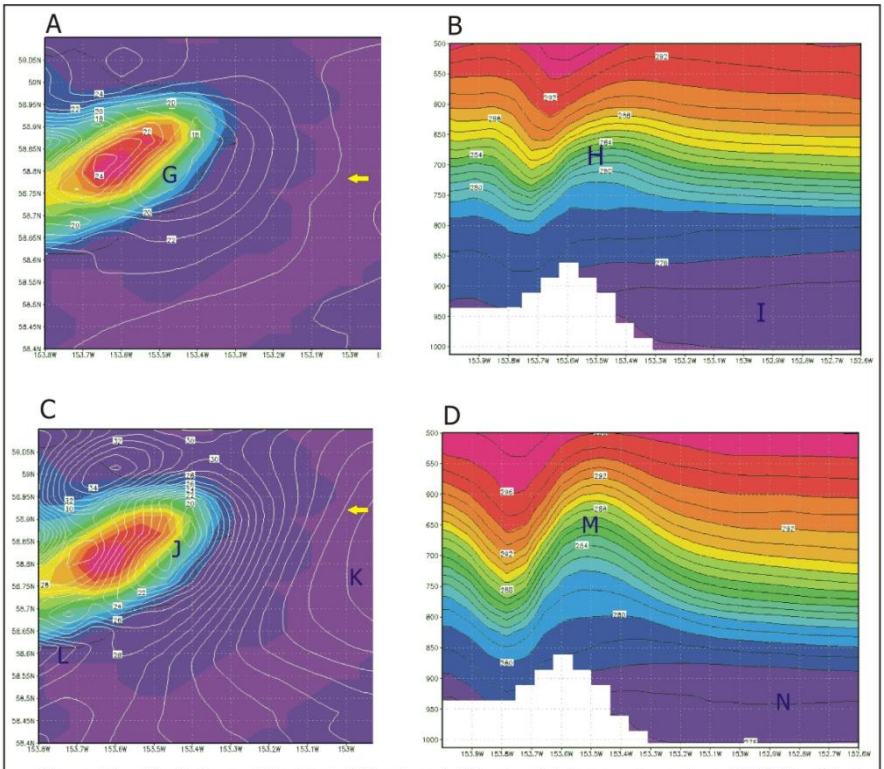

Figure A1: A) wind speed (m/s) at 950 mb and, B) potential temperature along 58.85N valid at 15Z Dec 27, 2006. C) wind speeds and, D) potential temperature valid at 21Z Dec 27.

The Fourpeaked Massif as represented in the model is approximately 1100 m high (~875 mb) with the long axis oriented from NE to SW. Figure A1 shows the 950 mb wind speeds (A & C) and east-west vertical cross-section's (B & D) of potential temperature six hours apart. There is a speed minimum of 18 ms^{-1} at 'G', diminished from a value of 25 ms^{-1} upstream near the yellow arrow in the top panel of Fig A1. Notice the modest amplitude mountain wave at 'H'. The troposphere at this

time is stable from 800 mb upward but neutral below as indicated at 'I'. Six hours later the speed minima at 'J' is on the order of 19-20 ms^{-1} however the upstream speed at 'K' is on the order of 37 ms^{-1}. As seen in the lower left panel of Fig A1, due to blocking the flow from 'K' to 'J' is diverted towards 'L', which is also seen in Figure A2 with 950 mb wind barbs. The flow at 'O' undergoes a reduction in speed but no change in direction; six hours later at 'P' however there is a prominent backing of the wind as it aligns itself parallel to the long-axis of the terrain. This pattern extends from the surface to approximately 1200 m (850 mb) where the winds start to veer back toward the east. Above the crest of the terrain there is a 700 m thick layer where the winds veer with height becoming easterly around 1800 m (775 mb); the terrain not only modifies winds upstream that are below the crest of the terrain, but winds directly above the terrain as well. Figure A3 shows the 950 mb geopotential heights at the two analysis times. Although the absolute height decreases from panel A to panel B, notice how the height difference to the east of the terrain (upstream) increases from 25 m to 50 m in response to the enhanced blocking. In effect the upstream reversed pressure gradient increases as the amplitude of the mountain wave increases.

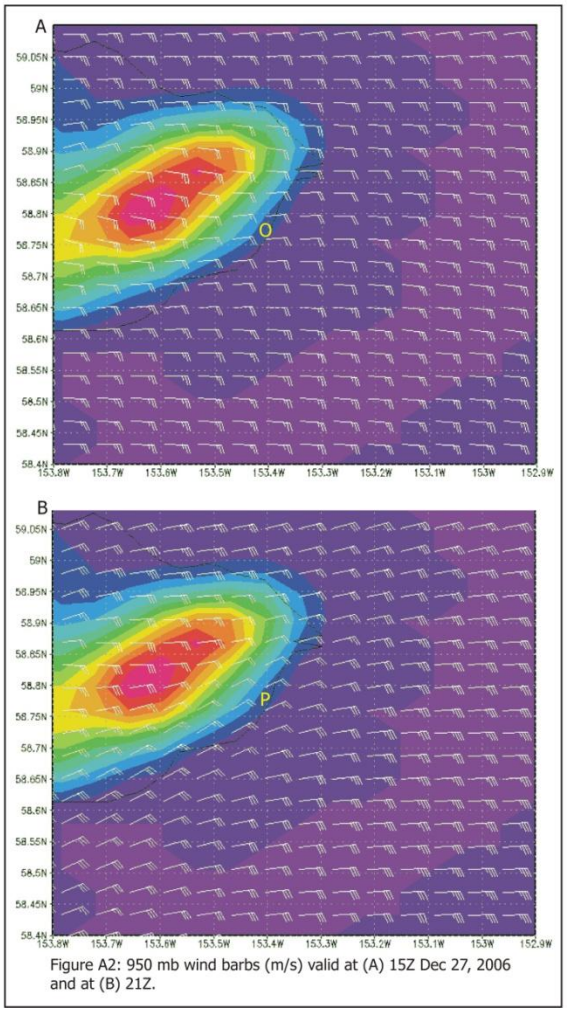

Figure A2: 950 mb wind barbs (m/s) valid at (A) 15Z Dec 27, 2006 and at (B) 21Z.

In this particular event the blocking that occurred <u>below</u> the crest of the Fourpeaked Massif which has been displayed in Figures A1-A3, is a function of leading edge of the mountain wave that is generated as strong easterly winds flow over the terrain. The vertical motion at 'M' in Fig A1 is on the order of 2-3 ms^{-1} which although not considered strong, it does generate enough lift to produce significant cooling in this layer. In addition there is no hint of wave breaking in the mountain wave; in other words this is a purely hydrostatic forcing as the leading edge of the mountain wave slowly migrates upstream in response to increased in stability and horizontal wind speed. Analysis of the vertical velocity field at various levels indicates that the area of rising motion expands upstream, with the highest values occurring in the 800-650 mb layer. It is also evident that the maximum in rising motion occurs at higher elevations with increasing upstream distance, in accordance with a quasi- stationary mountain wave with negative phase tilt. The time evolution of this wave indicates that there is little change in the tilt of a constant phase line, however not only does the amplitude of the wave increase but the width increases as well.

As noted above during the 6 hour period displayed in Fig A1 there is considerable warm air advection in northern Shelikof Strait associated with the LLJ and accompanying front. The actual air temperatures at 'M' increase some 2-3^{o} C compared to 'H'; however since air temperatures directly upstream has increased by some 6^{o} C during this interval, the column of air over the windward slope

experiences a relative cooling and hence produces higher pressure (heights) compared to its surroundings, as clearly evident in Fig A3 (Smith 1990). In fact the pressure gradient extending from the base of the slope to some distance upstream becomes negative by 17Z. Hence although blocking reaches a maximum in the layer <u>below</u> crest level, the dynamics that that makes it possible resides <u>above</u> the windward slope.

A layer-by-layer comparison of the Brunt-Vaisala frequency between 15Z and 21Z indicates a significant increase in stability in the 900-750 mb layer and a modest decrease in stability in the 750-650 mb layer. Had the surface-to-900 mb layer been stable then we would expect that a larger percentage of flow in this layer would at least initially flow upslope and cool; forming a low-level reservoir of cooler air in this region. Although only one example has been cited, there are a plethora of possible stability profiles that could be envisioned, for example if the layer below the crest of the terrain is stable but the layer directly above is considerable less stable, then a shallow blocked zone would form but would probably not be nearly as strong as the case presented in this section in which the stable layer is above the neutral layer. For any given terrain configuration there is a particular wind and stability profile that generates the most intense blocking and subsequent upstream deceleration. For severe low-level blocking it is critical to have a layer of high stability air residing near crest level and extending 1000 to 2000 m above. In the extreme case air becomes stagnate at some point on the windward slope and the flow reverses direction or moves parallel to the terrain.

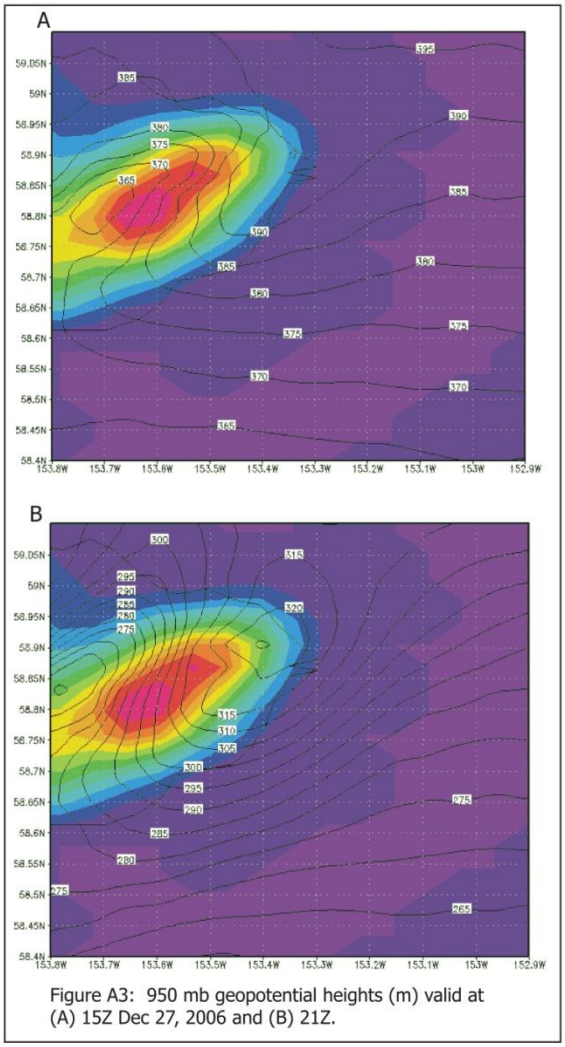

Figure A3: 950 mb geopotential heights (m) valid at (A) 15Z Dec 27, 2006 and (B) 21Z.

<u>References & Suggested Reading</u>:

Bond, NA., Macklin, S.A. 1993: Aircraft observation of offshore-directed flow near Wide Bay, Alaska. *Mon. Wea. Rev*. **121** 150-161.

Bond, N.A., Stabeno, P.J. 1998: Analysis of surface winds in Shelikof Strait, Alaska, using moored buoy observations. *Wea. & Forc*. **13** 547-559.

Durran, D.R. 1986: Another look at downslope windstorms. Part I: The development of analogs to supercritical flow in an infinitely deep, continuously stratified fluid. *Jr. Atmos. Sci*. **43** 2527-2543.

Gabersek, S., D.R. Durran. 2004: Gap flows through idealized topography. Part I: Forcing by large-scale winds in the nonrotating limit. Jr. Atmos. Sci. **61** 2846-2862.

Gabersek, S., D.R. Durran. 2004: Gap flows through idealized topography. Part II: Effects of rotation and surface friction. Jr. Atmos. Sci. **63** 2720-2739.

Lackmann, G.M., Overland, J.E. 1989: Atmospheric structure and momentum balance during a gap-wind event in Shelikof Strait, Alaska. *Mon. Wea. Rev*. **117** 1817-1833.

Liu, H., Olsson, P.Q., Volz, K.P., Yi, H. 2006: A climatology of mesoscale model simulated low-level wind jets over Cook Inlet and Shelikof Strait, Alaska. *Estu. Coast. Shelf. Sci*. **70** 551-566.

Overland, J.E. 1984: Scale analysis of marine winds in straits and along mountainous coasts. *Mon. Wea. Rev.* **112** 2530-2534.

Schar, C. 1993: A generalization of Bernoulli's theorem. *Jr. Atmos. Sci*. **50** 1437-1443.

Smith, R. 1990; Why can't stably stratified air rise over high ground? Appendix to Ch.5 in Atmospheric Processes over Complex Terrain. 105-107, AMS Pub. Vol.**23** no.45, Blumen- editor.

Smith, R.B. , A.C. Gleason., P.A. Gluhosky, V. Grubisic. 1997: The wake of St. Vincent. *Jr. Atmos. Sci.* **54** 606-623.

Young, G.S. and co-authors 2006: Synthetic aperture radar observations of mesoscale atmospheric phenomena. 14th Conference on satellite meteorology and oceanography. AMS conference February 2006. J4.7

Zangl, G. 2002: Stratified flow over a mountain with a gap: Linear theory and numerical simulation. *Q. J. R. Meteorol. Soc*. **128** 927-949.